Resonant x-ray and neutron diffraction study of $USb_{0.8}Te_{0.2}$

W.J. Nuttall, S. Langridge,* and W.G. Stirling
Physics Department, School of Physical Science and Engineering, Keele University, Keele, Staffordshire ST5 5BG, United Kingdom

G.H. Lander
European Commission, Joint Research Centre, Institute for Transuranium Elements, Postfach 2340, D-76125 Karlsruhe, Federal Republic of Germany

B. Lebech
Physics Department, Risø National Laboratory, DK-4000 Roskilde, Denmark

O. Vogt
Laboratorium für Festkorperphysik, Eidgenössische Technische Hochschule Zürich, CH-8093 Zürich, Switzerland
(Received 27 December 1994; revised manuscript received 5 May 1995)

Complementary neutron and magnetic x-ray scattering experiments have been performed on the pseudobinary compound $USb_{0.8}Te_{0.2}$. Both techniques reveal a succession of magnetic phases on cooling. On passing through the Néel temperature ($T_N \sim 205$ K), the system enters an antiferromagnetic (AF) state of modulation wave vector $q \sim 0.4$ reciprocal lattice units. Cooling further a second AF modulation ($q \sim 0.2$) appears which coexists with the $q \sim 0.4$ modulation over a narrow range of temperature. The appearance of the $q \sim 0.2$ scattering coincides with the onset of ferromagnetic ($q = 0$) order in the sample. The antiferromagnetic $q \sim 0.2$ modulation persists over a significant range of temperature in a mixed state with the emerging ferromagnetism. At the lowest temperatures studied, however, the system is found to be a saturated ferromagnet with no AF component. In the case of the x-ray study the onset of ferromagnetism is inferred from the concomitant distortion of the charge lattice. The smallest value of the magnetic peak width in the AF phase was always larger than the width of the neighboring lattice peak, consistent with finite-size effects in the ordered antiferromagnetism. Above T_N critical scattering is observed in the paramagnetic phase by both techniques. The x-ray critical scattering may be described by a single (Lorentzian) function corresponding to a single correlation length, in contrast to recent observations on several other systems. The results obtained in the neutron and x-ray experiments are compared and discussed.

I. INTRODUCTION

The use of x-ray resonant exchange scattering (XRES) for the study of magnetic structures and phase transitions has now become well established. XRES complements elastic neutron experiments as a second diffraction technique for the study of magnetic structures and correlations. The discovery by high-resolution neutron and/or x-ray techniques that the critical magnetic scattering of Ho,[1,2] Tb,[3,4] and the actinide compound NpAs (Refs. 5 and 6) apparently arises from two distinct length scales has raised the question of how widespread this phenomenon might be in magnetism. It challenges our understanding of second-order phase transitions, in which the ordering is conventionally understood to be driven by the divergence of the critical fluctuations. In this paper we report both neutron and synchrotron x-ray experiments on the magnetic structures and correlations of single crystals of $USb_{0.8}Te_{0.2}$. Perhaps surprisingly, in view of the earlier studies,[1,3,6] there is reasonable agreement between the neutron and x-ray results. The higher resolution of the x-ray technique revealed that the ordered antiferromagnetic (AF) state is more finite-size limited than the underlying lattice. Hints of such behavior are also visible in the neutron-scattering data and we discuss possible reasons.

USb is a well-studied uranium compound with a triple-q type-I antiferromagnetic structure developing at $\sim$ 212 K.[7] Doping with Te increases the ferromagnetic interactions (UTe is a ferromagnet) and the compound $USb_{0.8}Te_{0.2}$ (NaCl crystal structure, a=6.184 Å at room temperature) is a ferromagnet below $\sim$ 170 K. The $USb_{1-x}Te_x$ magnetic phase diagram[7–9] as a function of tellurium concentration, x, and temperature is shown in Fig. 1. For $x < 0.5$ the ordering temperature is fairly insensitive to composition (T_N = 213 K for USb) but gradually decreases to $T_C \approx 104$ K for pure UTe. All the solid solution compositions have continuous phase transitions.[8,9] For $x > 0.27$ the magnetic ordering is ferromagnetic with the moments lying along the $\langle 111 \rangle$ body diagonal. The saturated magnetic moment of the uranium atom has a value of $2.6\mu_B$ for $0.18 < x < 0.5$ and decreases to $1.9\mu_B$ in UTe.[8,9] The $\langle 111 \rangle$ easy axis is confirmed in the ferromagnetic phases by both the magnetization results and the presence of a rhombohedral distortion of the unit cell below T_C.[10] In the samples

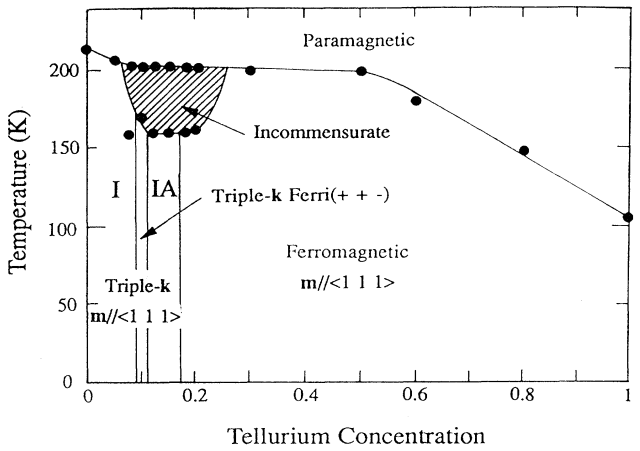

FIG. 1. The magnetic phase diagram of the solid solution $USb_{1-x}Te_x$ as a function of temperature and tellurium concentration. Modified from Ref. 7.

which are not purely ferromagnetic, the initial magnetic ordering occurs as longitudinal waves propagating along the fourfold cubic axes. The triple-q nature of the ordering assures that the resulting local easy axis is $\langle 111 \rangle$ in the AF compositions. The concentration dependence of the ordering wave vectors[8,9] near T_N is discussed by Burlet *et al.*[9]

II. EXPERIMENTAL DETAILS

The single crystals used in our diffraction studies were grown[11] at the ETH, Zürich, Switzerland. The sample used in the neutron experiment had a volume of 0.12 cm^3 and was mounted on a Cd shielded post with two orthogonally wrapped wires to reduce the use of adhesives containing hydrogen. The mosaic spread of this crystal as measured with the neutron spectrometer was 0.2° full width at half maximum (FWHM). The NaCl structure crystals cleave with $\langle 100 \rangle$ faces and a small piece from the same melt was used for the x-ray experiments. Its dimensions were $2 \times 4 \times 0.5$ mm^3. The mosaic width measured in the x-ray experiment was 0.07° (FWHM). It should be recognized that these measurements of the mosaic width reflect the convolution of the instrumental resolution with the true mosaic of the crystals.

The antiferromagnetic structures occurring in the cubic $USb_{1-x}Te_x$ series give rise to distinct satellite peaks in the diffraction experiments. These incommensurate modulations, of magnitude q, propagate along each of the six cubic fourfold symmetry directions. Our neutron-scattering experiment investigated the magnetic satellites of the (111) nuclear Bragg peak. The spectrometer was aligned such that the scattering plane coincided with that containing the (110) and (001) crystallographic reflections. In the case of the neutron-scattering experiment, the lowest angle magnetic satellites were those near the (111) Bragg peak. In particular $(1, 1, 1-q)$ and $(1, 1, 1+q)$ were accessible in the scattering plane. Our experiments concentrated on the former of these.

The neutron experiments were performed on the TAS1 triple-axis spectrometer, situated on the cold source of the Risø National Laboratory reactor. Operating in a two-axis mode, with the analyzer crystal removed, 5.08 meV neutrons were selected by a flat pyrolytic graphite (002) monochromator, with a cooled polycrystalline Be filter to remove higher order contamination. The collimation was $30' - 60' - 30'$. For the subsequent analysis of the critical scattering an accurate measurement of the resolution function was undertaken at the (111) nuclear Bragg peak at T=185 K. Gaussian fits to scans in the three symmetry directions yielded the following values, half-width at half maximum (HWHM): in-plane $\Delta q_{[001]} = 0.0063$ $Å^{-1}$ and $\Delta q_{[110]} = 0.0056$ $Å^{-1}$; the out-of-plane resolution width was 0.025 $Å^{-1}$.

In this paper we shall use the notation (Q_H, Q_K, Q_L) to denote the components of a general vector in reciprocal space defined with respect to the origin. The magnetic modulation wave vector defined with respect to a nearby reciprocal lattice point will be represented as being of magnitude q. In the neutron study the scattering cross section led us to investigate the magnetic satellites around (111), while in the x-ray study the constraints of reflection geometry dictated an investigation of the satellites of (002), four of which were accessible in-plane. Because of the different interactions in magnetic x-ray and neutron diffraction, the $(0, 0, 2+q)$ satellites of the (002) reflection have zero intensity in the neutron case. The study of different regions of reciprocal space in the two experiments leads us to introduce a simplified notation that facilitates direct comparison between the two experiments.

The fundamental magnetic properties may be described in terms of two reduced wave vectors, defined with respect to the direction of propagation of the magnetic modulation from a nearby reciprocal lattice point. We define $q_{\|}$ to be a wave vector along the direction of propagation, while $q_{\perp}$ denotes the wave vector component orthogonal to that. For symmetry reasons the scattering will be rotationally symmetric about the direction of propagation. In the case of our neutron study of the $(1, 1, 1-q)$ satellite the designation $q_{\|}$ refers to a wave vector along Q_L propagating from the (111) while $q_{\perp}$ corresponds to a wave vector in the in-plane direction [110].

The x-ray experiments were performed at beamline X22C of the National Synchrotron Light Source at Brookhaven National Laboratory. The beamline consists of a bent cylindrical nickel-coated focusing mirror and a Ge(111) double crystal monochromator that allows access to x-ray photons in the range 3.5 keV to $\sim$ 12 keV. As has been discussed in previous work[12,13] the use of resonant magnetic scattering enhancement in actinide systems requires photons ($\sim$ 3.7 keV) close to the low energy limit of the beamline. At these energies attenuation of the beam by air in the experimental hutch and by beryllium windows in the beamline is a significant concern and wherever possible evacuated flightpaths are used and the number of x-ray windows is kept to a minimum. All the magnetic x-ray scattering data presented here were obtained at the uranium M_{IV} edge using pho-

tons of energy 3.728 keV.[12,13] At this energy the $(1/e)$ penetration depth is of order 1500 Å. The sample geometry was defined such that the c direction was perpendicular to the largest face of the crystal which was centered in the x-ray beam. The sample was oriented such that the scattering plane coincided with the $Q_K = 0$ plane of reciprocal space.

When using XRES to extract critical exponents characteristic of these types of magnetic system it is essential to take rigorous account of the effects of instrumental resolution and crystal quality in the data analysis. Our data analysis methodology is based on that developed by Langridge *et al.*[5,6] The resolution ellipsoid is based on measurements from the (002) charge peak at 189.6 K with photons of energy 3.728 keV. We consider the intersection of the three-dimensional tilted resolution ellipsoid with the Cartesian axes of the reciprocal space. The cuts of the ellipsoid in these three directions yield the experimental resolution: in-plane $\Delta q_{[100]} = 0.00101$ Å^{-1}, $\Delta q_{[001]} = 0.00139$ Å^{-1} and out-of-plane $\Delta q_{[010]} = 0.0048$ Å^{-1} (HWHM); the [010] value was measured in a subsequent experiment on USb.[14]

In the x-ray experiments all four in-plane $q \sim 0.4$ magnetic satellites around (002) were observed. Our x-ray investigations of the ordered antiferromagnetic phases of $USb_{0.8}Te_{0.2}$ involved a study of both the (0, 0, 2+q) and (q, 0, 2) magnetic satellites. We note that the designation $q_{||}$ would in the former case refer to a wave vector in the Q_L direction. In the latter case $q_{||}$ would denote a wave vector along Q_H. In each case $q_\perp$ would describe the orthogonal wave vector in the $Q_K = 0$ plane. Our critical scattering data were taken from the most intense of the four observed satellites, that at (0, 0, 2 + q).

III. NEUTRON-SCATTERING RESULTS

A. Magnetic phase diagram

Consistent with the earlier neutron work[8,9] on $USb_{0.8}Te_{0.2}$, the neutron experiments have detected four phases between T_N and low temperature. These regimes are illustrated in the top panel of Fig. 2. Above $T_N \sim 205$ K the system is paramagnetic. On cooling through T_N the system enters an incommensurate AF phase with modulation wave vector $q \sim 0.4$. On cooling further towards the Curie temperature $T_C \sim 175$ K the situation becomes somewhat more complicated. A second ($q \sim 0.2$) AF modulation appears and coexists for a narrow range of temperature with the now diminishing $q \sim 0.4$ feature. Accompanying the growth of the $q \sim 0.2$ phase is the onset of a ferromagnetic ($q = 0$) component, measured, for example, at the (111) point. At the lowest temperatures (below about 145 K) only the saturated ferromagnetic $q = 0$ component remains.

In Fig. 3 we show representative $q_{||}$ scans through the magnetic (1, 1, 1 − q) satellites of (111). For all of the $USb_{1-x}Te_x$ structures examined neutron-scattering studies find no satellites along the [001] direction itself;[8,9] this indicates that the magnetic Fourier components are longitudinal in nature, as any component transverse to the direction of the momentum transfer would give rise to satellite reflections. A further insight into the magnetic structure is illustrated in the inset to Fig. 3. This feature is the third harmonic of the magnetic modulation. A true AF square-wave spin structure in real space would be expected to generate all odd Fourier components in reciprocal space. It is clear from the existence of this third harmonic signal that the incommensurate AF magnetic modulation of $q \sim 0.2$ is not sinusoidal in form but that there is a strong tendency to "squaring."

The wave vectors of the AF components are shown as a function of temperature in the middle panel of Fig. 2. The discontinuity in wave vector at about 175 K corresponds to a first-order phase transition. The onset of ferromagnetism illustrated in the top panel of Fig. 2 is

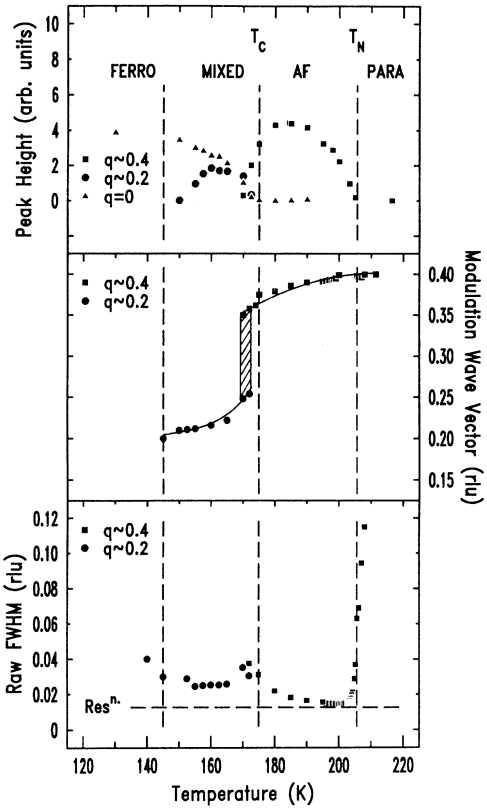

FIG. 2. Top: Temperature dependence of the neutron-scattering magnetic peak intensity for the antiferromagnetic and ferromagnetic ordering. The ferromagnetic intensity has been reduced by a factor of 10 to be on the same scale as the antiferromagnetic intensities. Middle: The antiferromagnetic ordering wave vector as a function of temperature. The hatched area represents the approximate extent of the region of coexistence. The curves are guides to the eye. Bottom: The width of the $q_{||}$ antiferromagnetic scattering observed in the neutron experiment. Note the critical broadening above T_N and the slower increase in width away from T_N in the ordered phases. The T_N illustrated is as determined from the data in Fig. 4. The horizontal dashed line represents the appropriate experimental resolution.

associated with the appearance of the $q \sim 0.2$ modulation in coexistence with the $q \sim 0.4$ signal. This coexistence of the two AF modulations is shown by the scans at 170 K and 171 K in Fig. 3. Intuitively the simplest explanation is that the two antiferromagnetic modulations relate to different magnetic phases which coexist in different parts of the sample. It is important to state that the appearance of the $q \sim 0.2$ modulation is clearly related to the onset of ferromagnetism in the sample. It is natural therefore to assume that the $q \sim 0.2$ AF modulation exists in that portion of the sample with ferromagnetic alignment. The coexistence region would therefore consist of two spatially separated parts of the crystal. The first, essentially ferrimagnetic, would consist of a superposition of $q = 0$ and $q \sim 0.2$ modulations while the second would consist of the residual volume fraction in the $q \sim 0.4$ state. As shall be discussed in Sec. IV C the onset of the ferromagnetism is associated with a rhombohedral distortion of the crystal lattice. This structural distortion may be responsible for favoring the $q \sim 0.2$ modulation of the antiferromagnetism. Below 145 K there is no sign of any AF ($q \neq 0$) component and the system as a whole may be regarded as a saturated ferromagnet.

These magnetic structure results are similar to those reported by Burlet *et al.*[8,9] for samples with a nominally equivalent composition to our own. They indicate also that the phase diagram, Fig. 1, is more complicated near the ferro/antiferromagnetic boundary. Similar complicated phases have been found in $U_{0.85}Th_{0.15}Sb$ by Paixão *et al.*[15] This latter paper discusses in detail the difficulties of interpreting these different Fourier components, and hence obtaining an understanding of the actual real-space magnetic structure. We note that similar coexistences have been observed in the multiply commensurate monopnictide antiferromagnet CeSb.[16] In this case also it is far from trivial to determine the precise real-space magnetic structures from the observed neutron-diffraction data.

In the bottom panel of Fig. 2 we illustrate the behavior with temperature of the width of the antiferromagnetic satellites. Above T_N there is a rapid broadening of the magnetic peak corresponding to critical fluctuations within the paramagnetic phase. The critical scattering will be discussed in Sec. III B. From Fig. 2 we see that the $q \sim 0.4$ satellite peak is sharpest just at T_N. We note that the (raw) width (FWHM) of this feature is ~ 0.014 r.l.u. (0.014 Å^{-1} as $2\pi/c = 1.016$) at T_N. This is slightly broader than the experimental resolution of 0.0126 Å^{-1} in that direction. It is noteworthy that the neutron widths in the $q \sim 0.4$ ordered AF phase increase slightly on cooling. This result will also be discussed in Sec. IV A in the context of the x-ray observations.

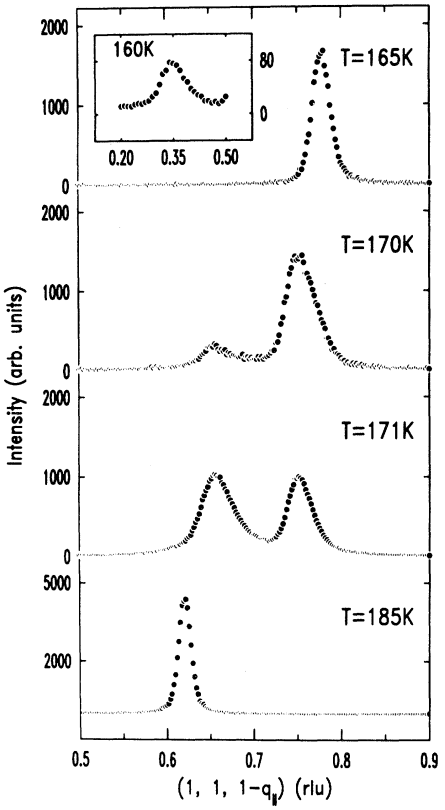

FIG. 3. Representative neutron data in the AF and mixed phases. The two middle scans illustrate the coexistence of $q \sim 0.2$ and ~ 0.4 modulations. The inset (T =160 K) shows the third harmonic of the $q \sim 0.2$ modulation. The x-axis numbering corresponds to the values of $(1-q_{\|})$.

B. Critical region

Published data[8,9] on $USb_{0.8}Te_{0.2}$ give an ordering temperature of $T_N \approx 205$ K. For a detailed investigation of the critical phenomena an accurate determination of the ordering temperature is required. The cusp in the magnetic intensity measured at $(0.986, 0.986, 0.6)$ gave $T_N = 205.3 \pm 0.4$ K. Using this estimate a more refined investigation was made of the integrated intensities near T_N. Figure 4 shows the integrated intensity of the $(1, 1, 0.6)$ magnetic satellite as a function of temperature. Fitting the data to a power law function of the reduced temperature $t = (T - T_N)/T_N$, given by

$$I = I_0|t|^{2\beta} \tag{1}$$

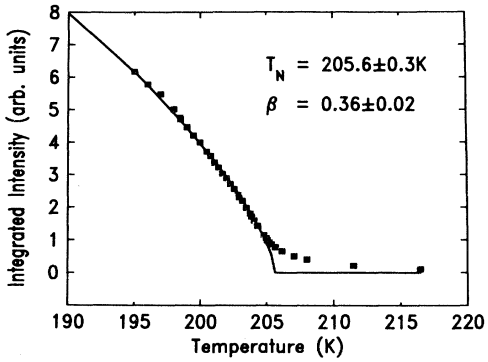

FIG. 4. The integrated neutron intensity of the $(1, 1, 0.6)$ magnetic satellite. The solid curve is a power law fit discussed in the text.

gives an ordering temperature of $T_N = 205.6 \pm 0.2$ K and a sublattice magnetization exponent of $\beta = 0.36 \pm 0.02$, which is in agreement with the three-dimensional (3D) Heisenberg value of 0.367. Symmetry arguments[17] have been advanced to place the $USb_{0.8}Te_{0.2}$ system in a universality class with an order parameter described by a six component vector. For this class, anisotropy in the Hamiltonian does affect the observed exponents, although not too significantly, with the result that the predicted exponents are similar to the 3D Heisenberg model.

Figure 5 illustrates representative critical scattering data obtained in the paramagnetic phase, measured around the reciprocal space position $(1, 1, 0.6)$. The data clearly indicate broadening associated with critical fluctuations of the magnetic correlations above T_N. In this critical regime, a simple anisotropic Lorentzian function centered at $q \sim 0.4$ was found to be adequate to describe the isothermal staggered susceptibility;

$$\chi(\mathbf{Q}) = \frac{\chi(0)}{1 + (q_\perp/\kappa_\perp)^2 + [(q_\parallel - q)/\kappa_\parallel]^2}\ ; \quad q_\parallel = 1 - Q_L,$$

$$q_\perp^2 = (Q_H - 1)^2 + (Q_K - 1)^2, \tag{2}$$

where $\kappa_\parallel$ and $\kappa_\perp$ are the inverse correlation lengths parallel and perpendicular to the ordering wave vector (0, 0, $-q$).

As shown in Fig. 5 the scattering in the transverse direction [110] is approximately four times narrower than the [001] longitudinal scattering reflecting the real-space anisotropy in the exchange interaction.[7] The values for $\kappa_\parallel$ and $\kappa_\perp$ were obtained from a three-dimensional convolution of the critical scattering, modeled as an anisotropic Lorentzian [Eq. (2)] with a tilted ellipsoid corresponding to the experimental resolution; due account was taken of the small background contribution to the scattering. These fitted values are shown in Fig. 6. It is important to note that the Néel temperature emerging from our fits to the critical paramagnetic data (204.66±0.13 K) is slightly lower than that determined from the decay of the ordered phase magnetization (205.6 K±0.2 K). Similar effects have recently been reported for resonant magnetic x-ray experiments on holmium.[1,2] The anisotropy $\kappa_\parallel/\kappa_\perp$, illustrated as a function of temperature in the lower panel of Fig. 6, is approximately constant with temperature and has a value of $R = 4.25 \pm 0.50$. The solid lines in the upper panel of Fig. 6 correspond to a fit of the form $\kappa = \xi^{-1} \sim |t|^\nu$ applied to both the neutron data presented here and to the x-ray data discussed in Sec. IV B. We note that this conventional power-law form for κ assumes a divergence at T_N (i.e., $\kappa \to 0$) which is not in fact observed experimentally. The exponent $\nu = 0.46$ arises from a simultaneous fit to the four data sets: longitudinal and transverse scattering as measured with neutrons and x rays. The data have only

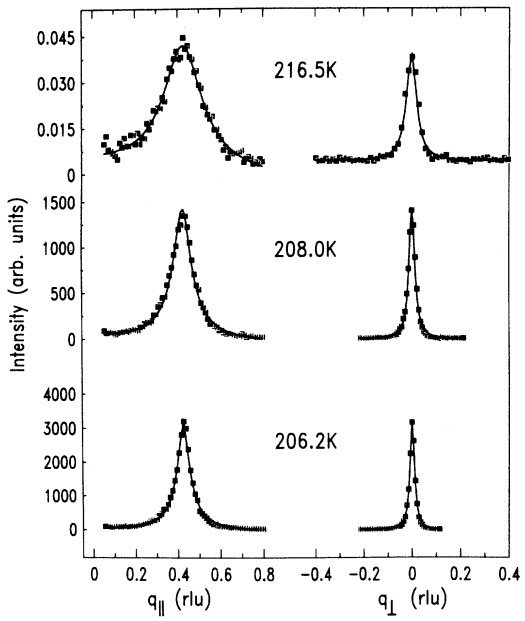

FIG. 5. Critical neutron scattering from $USb_{0.8}Te_{0.2}$ around $(1, 1, 0.6)$ in the [001] ($q_\parallel$) and [110] ($q_\perp$) directions. The solid curves are least-squares fits to the isothermal susceptibility folded with the three-dimensional resolution function. The instrumental resolution widths (FWHM) are $\Delta q_\parallel \sim 0.013$ Å^{-1} and $\Delta q_\perp \sim 0.011$ Å^{-1}.

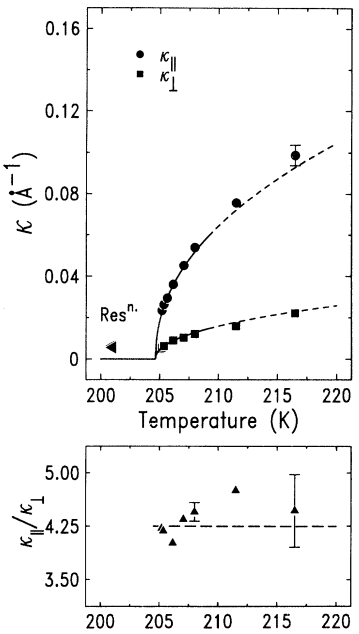

FIG. 6. A plot of the inverse correlation lengths $\kappa_\parallel$ and $\kappa_\perp$ as a function of temperature (neutron data). The curves drawn correspond to power law fits to both the neutron values shown here and the x-ray results illustrated in Fig. 12. The curves correspond to a critical exponent $\nu = 0.46$ and are drawn with a solid line over the range of the fit. The power law fit assumes $\kappa = 0$ for $T < T_N$. Such a conventional approach represents an approximation in this case as the system does not long-range order at T_N. The lower panel illustrates the behavior of the anisotropy with temperature. The dashed line corresponds to the weighted mean value.

been fitted over a range of reduced temperature ($t < 0.022$), that is, in the neutron case, up to a maximum temperature of 209.2 K. Fitting over this range, denoted by the solid curve in Fig. 6, allows a consistent treatment of both the neutron and x-ray data while excluding those points of poorest statistical reliability. Despite the high statistical quality of the neutron data the observed value of the correlation length critical exponent ν is unusually small. The values obtained from fits to the neutron data alone are longitudinally $\nu = 0.442 \pm 0.014$ and transversely $\nu = 0.435 \pm 0.012$ (for $t < 0.022$). These values are inconsistent with most universality classes of critical phenomena with the possible exception of mean field,[18] for which $\nu = 1/2$. There is, however, little physical justification for a mean field description of this system. We return to the discussion of the critical exponent ν in Secs. IV C and V.

IV. X-RAY SCATTERING RESULTS

A. Phase diagram

The technique of x-ray resonant exchange scattering (XRES) can be used to determine a magnetic phase diagram just as is the case with neutron scattering.[1–6] There are, however, certain limitations that are specific to the use of x rays. In particular, no direct observation of the ferromagnetic signal is possible with the XRES technique, as performed in our study. This is a consequence of the ferromagnetic signal being superimposed on top of the far brighter charge scattering from the crystal lattice. As we shall discuss later in Sec. IV C an indirect measurement of the onset of ferromagnetism may be possible with x-rays as a consequence of the high q resolution attainable. In the case of $USb_{0.8}Te_{0.2}$ the Curie temperature is clearly visible through the magnetoelastic distortion of the charge lattice that is associated with the appearance of ferromagnetism.

In the top panel of Fig. 7 we illustrate the relative contributions of the various magnetic modulations observed in our x-ray study, in an analogous way to the neutron results presented in Fig. 2. As in the neutron case we observe the growth of an ordered AF phase below T_N with a modulation wave vector of $q \sim 0.4$. Similarly, on cooling further we also observe a discontinuous phase transition to a state including a $q \sim 0.2$ modulation. Figure 8 illustrates representative data from the ordered AF phases below T_N analogous to the data presented earlier in Fig. 3. In contrast to the neutron case the x-ray results show no indication of any higher order Fourier harmonics of the magnetic structure. Discrepancies in observations of higher harmonics between neutron and x-ray studies of actinide antiferromagnets have been previously considered to be a consequence of the small x-ray penetration depth.[15,19]

The resolution of the x-ray technique provides evidence towards an explanation of the broadening of the $q \sim 0.4$ modulation peak at low temperatures observed in the neutron experiment and illustrated in Fig. 2. From Fig. 8 we see clearly that near the Curie temperature ($T \sim 185$ K) the x-ray data at higher q in fact correspond to several discrete modulation wave vectors. At higher temperatures closer to T_N there is evidence of only a single modulation wave vector which is seen to move smoothly with temperature, implying truly incommensurate behavior. The existence of several discrete $q \sim 0.4$ modulations is clearly suggestive of higher order commensurate values as are observed in "devil's staircase" systems such as CeSb.[20,21]

In the middle panel of Fig. 7 we present x-ray results illustrating the behavior of the modulation wave vector. The form and symmetry of the magnetic modulations as a function of temperature are similar to those observed in our neutron investigation (Fig. 2). The only differ-

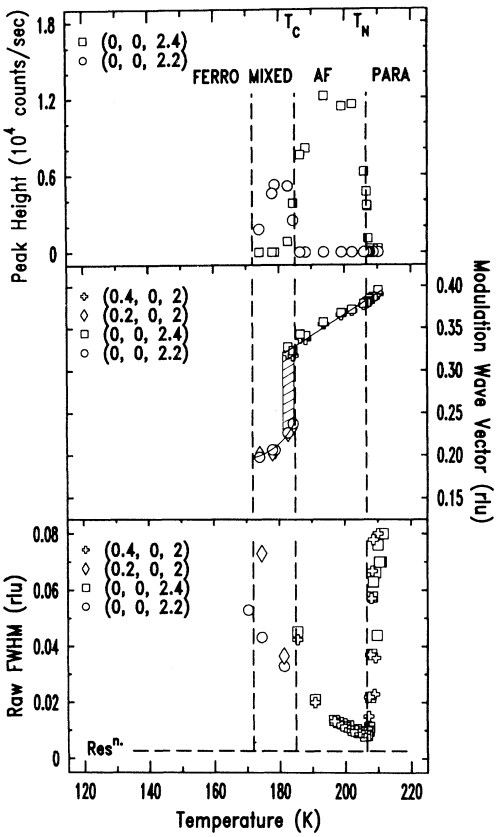

FIG. 7. Top: Relative intensities of the various AF modulations ($q \sim 0.2$, $q \sim 0.4$) observed in our XRES study at (0, 0, 2+q). Information from the low temperature ferromagnetic phase was not directly available from the x-ray technique. Middle: The antiferromagnetic ordering wave vector as a function of temperature. Data presented have been collected at the (0, 0, 2 + q) and (q, 0, 2) satellites. The hatched area represents the approximate extent of the region of coexistence. The curves are guides to the eye. Bottom: The widths of the $q_{||}$ magnetic x-ray scattering as a function of temperature. Note the critical broadening above T_N and the significant increase in width away from T_N in the ordered phases. The horizontal dashed line represents the resolution in the Q_L direction. A similar but slightly sharper resolution applies in the Q_H direction.

ence between the two results is that in the x-ray study we observe the coexistence of the two modulations to set in at a higher temperature, ~185 K, rather than the ~175 K observed in the neutron study. This discrepancy results from the correspondingly different values of the Curie temperature observed by the magnetic neutron diffraction and the x-ray study of the lattice distortion discussed in Sec. IV C.

As noted in Sec. I the x-ray sample represented a very small part of the original melt. The small near-surface volume probed by the x rays might be expected to have a slightly different stoichiometry than the average across the large crystal sampled in the neutron study. Small differences in the effective tellurium concentration between the neutron and x-ray experiments may partly be responsible for the differences in observed Curie temperatures T_C. As illustrated in Fig. 1, T_C has a stronger dependence on tellurium concentration (x) than the Néel temperature T_N. In the x-ray experiments we find a consistency between T_C inferred from the onset of the $q \sim 0.2$ modulation measured with 3.728 keV x rays and the value obtained from the lattice distortion measurements obtained with 8 keV photons and discussed in Sec. IV C. As such there is little evidence for unusual effects associated with the extremely small near-surface volume probed with the 3.728 keV x rays in the XRES study when compared to the deeper sample penetration obtained at 8 keV. However, the full extent of the role of the surface in determining measured magnetic properties is not yet well established and will await a comparison of the x-ray measurements with surface-sensitive high-resolution neutron diffraction. Recently an experiment has been reported by Gehring and co-workers in which a tightly collimated neutron beam was used to probe antiferromagnetic ordering in the near-surface region of a terbium single crystal.[3,4] They report that the near-surface "skin" is found to have a narrower critical scattering line shape than the bulk and that the skin extends to a depth of ~ 0.2 mm, which is significantly larger than the penetration depth in a typical actinide XRES study.[6]

In the lowest panel of Fig. 7 we illustrate the behavior of the widths of the antiferromagnetic peaks, where we have treated the $q \sim 0.4$ modulation as a single feature despite the evidence for discrete structure, mentioned earlier. There is a similarity between these observations and those presented earlier in Fig. 2. In the x-ray case, however, the broadening of the antiferromagnetic scattering is more pronounced and more rapid with decreasing temperature than was seen with the neutrons. Both techniques gave the smallest width for the $q \sim 0.4$ modulation just below T_N. In each case the data shown represent raw values without consideration of instrumental resolution. For both the x-ray and neutron experiments the raw values of the peak width at T_N appear larger than the experimental resolution implying an absence of true long-range order in the system. The essential features of this result are confirmed, although less dramatically, by the more rigorous analysis associated with the critical scattering and discussed in Sec. IV B.

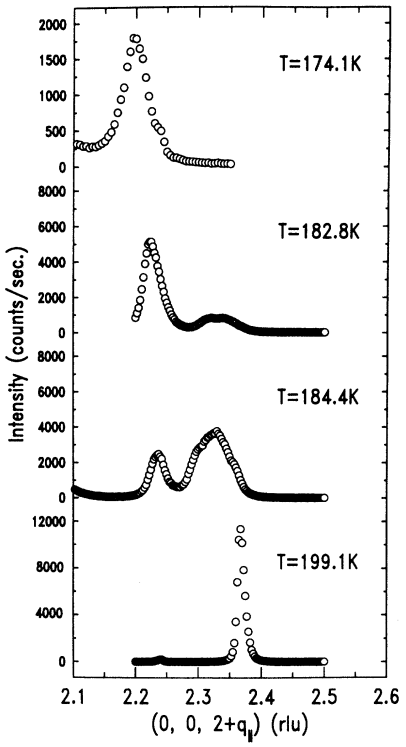

FIG. 8. Representative x-ray data in the AF and mixed phases. The middle scans illustrate the possibility of three or more coexisting modulations at higher q coexisting with the $q \sim 0.2$ modulation. The small feature ($\sim$ 500 counts/sec) at $q_{\|} = 0.24$ visible in the 174.1 K and the 199.1 K data is part of the background measured at 225.3 K. The x-axis numbering corresponds to the values of $(2+q_{\|})$.

B. Critical regime as measured by x rays

Figure 9 shows a power law fit [Eq. (1)] to the integrated intensity obtained from $q_{\|}$ scans through the (q, 0, 2) peak. The measured XRES intensity has been assumed here to arise purely from the magnetic two spin

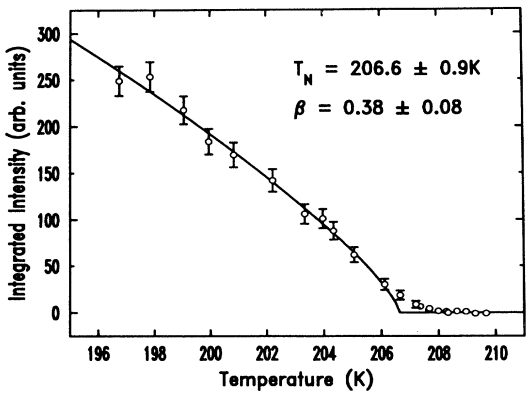

FIG. 9. The integrated x-ray intensity of the (0.4, 0, 2) magnetic satellite. The solid curve is a power law fit discussed in the text.

correlation function. Recent theoretical work has lent support to this assumption in those cases where the experimental energy resolution is sufficiently broad as to regard the scattering as quasielastic.[22] These and similar considerations have been discussed recently by Thurston *et al.*[2] Therefore, we have fitted the measured integrated intensity to Eq. (1) in a manner directly analogous to that used to analyze the neutron data presented in Fig. 4. The fit obtained is shown in Fig. 9; a value for the critical exponent β of 0.38 $\pm$ 0.08 is obtained, in agreement to within error with the value observed in our neutron-scattering experiment. The corresponding value of the Néel temperature, T_N, is 206.6±0.9 K. This compares with our measurement of T_N in our order-parameter neutron investigations of 205.6 K and a published value of 205 K from Burlet *et al.*[8,9]

Broad scattering peaks arising from the critical fluctuations in the paramagnetic phase were observed at both the (*q*, 0, 2) position and the (0, 0, 2+*q*) position. In the latter case critical scattering was observable at temperatures up to $T_N + 7$ K. Just as in the case of the neutron data the model line shape for the critical scattering was taken to be an anisotropic Lorentzian [Eq. (2)]. In this case, however, at (0, 0, $2+q$) we note that $q_{\|} = Q_L - 2$, and $q_{\perp} = Q_H$. The measured background (at 225.3 K) was subtracted from the data prior to analysis with a convolution of the model line shape and experimental resolution. This ensured that the analysis treated only the symmetric and distinct peak associated with the (0, 0, 2+*q*) AF modulation and was not affected by the tails of the (002) charge peak which appears as a sloping background in the raw data.

In Fig. 10 we present representative, background subtracted, data from the critical paramagnetic phase above T_N as measured at the (0, 0, 2+*q*) peak. The rapid decrease in intensity (static staggered susceptibility) and the smooth broadening of the diffraction signal both longitudinally and transversely is clearly indicative of critical scattering and are consistent with a continuous phase transition. In contrast to previous XRES studies of critical scattering[1–6] we find that a single anisotropic Lorentzian is sufficient to obtain excellent fits to the data, as illustrated in Fig. 10. There is no need to invoke a "two-component" line shape as has been required previously for other systems.[1–6]

The critical scattering synchrotron x-ray results are summarized in Fig. 11 in a form analogous to that used for the neutron results of Fig. 6. As in the neutron case we find that the value of the Néel temperature obtained from the critical scattering (207.4±2.3 K) is slightly different than that arising from the ordered phase data. However, in this case the discrepancy is well within error. As in the neutron study values of the correlation length exponents may be extracted from the critical scattering data. However, in the x-ray case the greater scatter of the observed κ values prevents a precise determination of the correlation length exponent based upon the x-ray measurements alone. In Fig. 11 we illustrate the κ values obtained from our fits to the x-ray scattering data. It is immediately apparent that these data lie in a similar range to those obtained with the neutron scattering and illustrated in Fig. 6. That is, the inverse correlation lengths extracted from our Lorentzian line shape correspond to the same critical fluctuations as have been seen with the neutrons in this study. As such the x-ray critical scattering is reminiscent of the broader component in the "two-component" line shapes reported for other systems. The solid curve in the upper panel illustrates the $\nu = 0.46$ dependence obtained in a simultaneous fit to all the measurements both neutron and x ray and illustrated earlier in Fig. 6. The dashed curve extends this power law dependence beyond the range of the fit ($t < 0.022$). The x-ray results summarized in Fig. 11 are remarkably consistent with the neutron-diffraction results (Fig. 6). A fit to the x-ray results alone yields in the parallel direction $\nu \sim 0.75$ while in the perpendicular direction $\nu \sim 0.65$ in each case the uncertainty is so large ($\sim \pm 0.5$) that little physical understanding can be obtained from these nominal values. In the lower panel of Fig. 11 the measured anisotropy of the extracted widths is illustrated. The x-ray result clearly shows more scatter than the neutron result but is consistent with the neutron value.

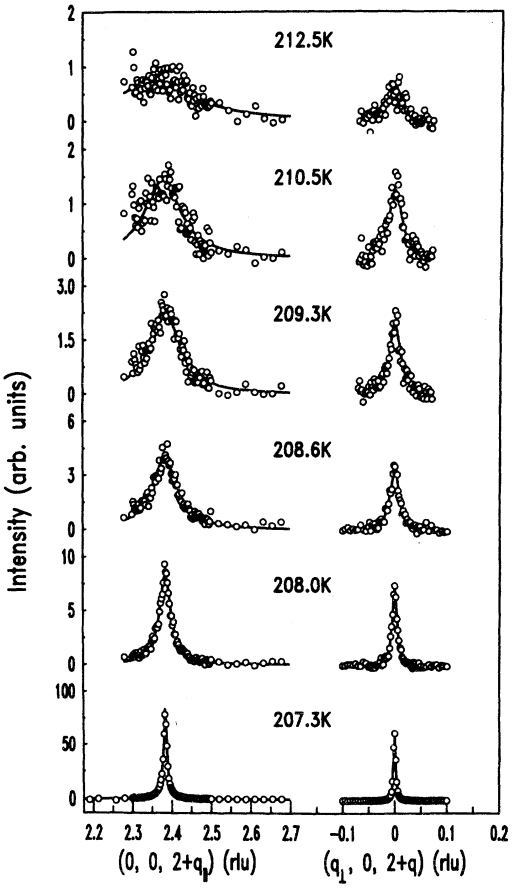

FIG. 10. Critical x-ray scattering around (0, 0, $2+q$). $q_{\|}$ denotes the Q_L direction while $q_{\perp}$ corresponds to Q_H. The solid curves are least-squares fits to an anisotropic Lorentzian folded with the three-dimensional resolution function. The experimental resolution widths (FWHM) are $\Delta q_{\|} \sim 0.00279$ Å^{-1} and $\Delta q_{\perp} \sim 0.00203$ Å^{-1}.

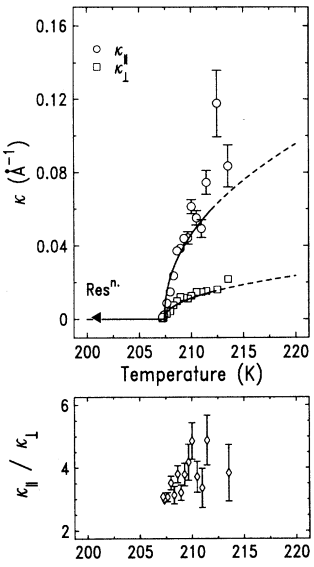

FIG. 11. A plot of the inverse correlation lengths $\kappa_{\|}$ and $\kappa_{\perp}$ as a function of temperature (x-ray data). The values derive from data obtained at the (0, 0, 2 + q) satellite. The curves correspond to the $\nu = 0.46$ fit to all the inverse correlation length data, as illustrated previously in Fig. 6. In the x-ray case the residual width at T_N as determined from the convolution routine is slightly smaller than would be indicated by the raw data illustrated in Fig. 7. By both measures, however, the $q_{\|}$ data reveal an excess width corresponding to a lack of long-range order at T_N. The lower panel illustrates the behavior of the anisotropy with temperature.

C. High resolution x-ray study of lattice behavior

The position and width of the (002) and (004) charge peaks have been determined as a function of temperature using 8 keV photons and a Ge(111) analyzer to improve the instrumental resolution. We show in Fig. 12(a) the variation of the d_{001} lattice spacing as measured from both the (002) and (004) charge peaks as a function of temperature. In the paramagnetic ($T > T_N$) and antiferromagnetic phases ($T > 185$ K) d_{001} is identical to the lattice parameter. For both reflections studied there is a large anomaly at T_C. There is no indication of any discontinuous behavior in the lattice at T_N that would be indicative of weakly first order Néel transition. Below T_C the onset of magnetoelastic stress causes the d_{001} spacing to reach a maximum at $\sim$ 150 K. Below T_C d_{001} is no longer strictly the lattice parameter because a rhombohedral distortion occurs.[10] Hulliger and Vogt reported a lattice distortion, which results in an elongation along the ⟨111⟩ diagonal with an accompanying change of the cubic angle from 90° to 89.85°. We cannot, of course, determine both the parameters (length and angle) of the rhombohedral distortion by measuring only one set of charge peaks, but our results for the increase of d_{001} are consistent with their measurements.[10] In their sample T_C was 158 K, but the stoichiometry may have been slightly different from the present sample. The present neutron experiments give $T_C = 175$ K, whereas the x-ray experiments find $T_C = 183$ K. A similar expansion of the d_{001} spacing at T_C was found in $U_{0.85}Th_{0.15}Sb$ by Paixão *et al.*[15]

We have also measured both the longitudinal and transverse widths of the (002) and (004) charge peaks as a function of temperature, and the results are shown in Fig. 12(b). The longitudinal widths show no variation throughout the temperature range and have a value corresponding to $\Delta Q_L/Q_L = 5 \times 10^{-4}$. This is again consistent with a rhombohedral distortion, which does not change the equivalence of the d_{001} plane spacings. However, the transverse widths show an unusual change below T_C. The width of the (002) reflection changes much more than that of the (004). Strain arguments require that these changes be either equivalent, or that there is a linear Q dependence, rather than the observed in-

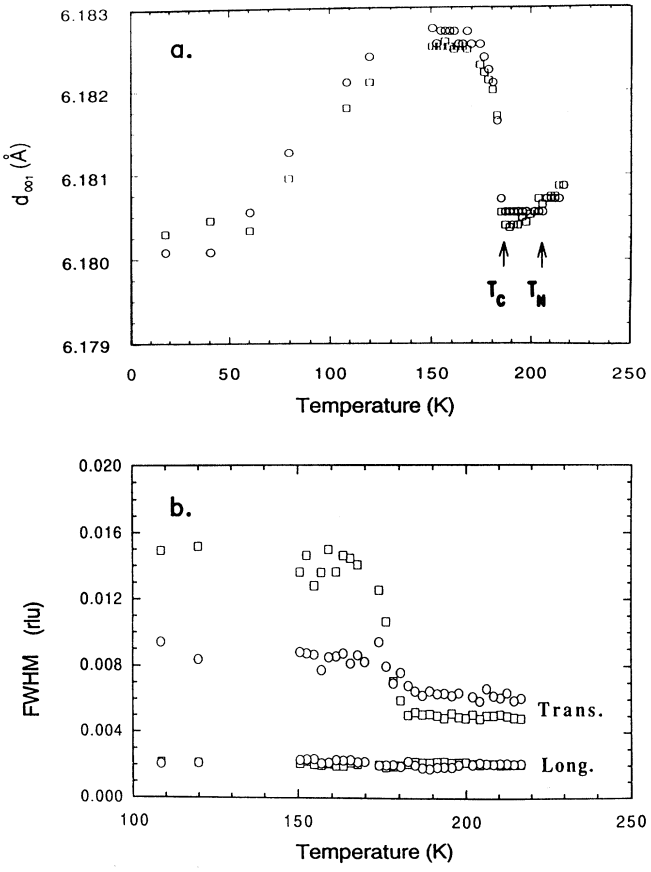

FIG. 12. (a) Variation of the d_{001} lattice spacing with temperature (high resolution x-ray data). The squares are from the (002) charge peak and the circles are from the (004). The relative changes in d_{001} are well established although the absolute value may be subject to significant systematic error. (b) Variation of the parallel and transverse widths (FWHM) of the (002) (□) and the (004) (○) charge peaks. The ordinate axis is correct for the (004); the values given for the (002) have been doubled. Dividing the ordinate values by 4 gives $\Delta Q_L/Q_L$ for the longitudinal scans, and the width in radians for the transverse scan.

verse proportionality with momentum transfer, Q. Such an unusual Q dependence was also found below T_C by Paixão *et al.*[15] in $U_{0.85}Th_{0.15}Sb$. These authors proposed that this could be interpreted as arising from a depth-dependent mosaicity resulting from reorientation of the crystallites due to the rhombohedral distortion.

V. DISCUSSION

The x-ray experiments reported here were undertaken to examine more carefully the nature of the critical scattering line shape. To our surprise, no evidence for a second "sharp" component has been observed, in contrast with reports from previous studies on Ho,[1,2] Tb,[3,4] and NpAs.[5,6] More recently such a sharp component has been found also in USb,[14] so that the systematics of this situation remain unclear. Of course, a small amount of the sharp component would be difficult to detect, particularly as this contribution is normally[2,4,5,14] only observable relatively close to T_N. We note that the neutron critical scattering data are far superior to those obtained for NpAs,[23,24] because of absorption by Np and the limited crystal size of transuranium materials.

The origin of the second sharp component is still controversial, with defects in the "skin" region being presently favored.[4] Near-surface defects have been invoked to explain the observation of long-range magnetic order in the random field Ising antiferromagnet $Mn_{0.75}Zn_{0.25}F_2$, for temperatures and fields at which the bulk exhibits short-range order.[25,26] It is interesting to note that no special precautions were taken in the experiments reported in this paper to prevent the formation of an oxide overlayer. Further the crystal quality is certainly no better than either NpAs (Refs. 5 and 6) or USb,[14] in both of which strong sharp components have been seen near T_N. In the experiment reported here the magnetic critical scattering does not sharpen up to a value equivalent to the experimental resolution. This implies therefore that the AF phases are not truly long-range ordered and below T_N the correlations are always finite-size limited. A similar situation was found in the $U_{0.85}Th_{0.15}Sb$ system by Paixão *et al.*[15] but unfortunately no measurements of the critical scattering were reported in that study. We have some indication from the x-ray data that the ordered phase magnetic correlations are somewhat anisotropic, with a minimum value of $R \sim 2.5$ for temperatures just below T_N. Cooling further the anisotropy increases consistent with the $q_{||}$ broadening illustrated in the lowest panel of Fig. 7. A full understanding of these properties, however, will await further x-ray experiments performed at very high q resolution with an analyzer crystal. Such experiments would allow for a precise determination of both the finite-sized limit to the AF correlations at T_N and the anisotropy.

To summarize, the experiments reported here have shown two unusual effects. The first is the absence of any observable sharp component in the critical scattering, and the second is that the magnetic correlations never diverge to infinity (as defined by the lattice periodicity). The smallest inverse correlation lengths are observed just below T_N. Although we observe that the x-ray data never reach the resolution limit a precise quantitative study of the finite-sizing of the ordered phase will await higher resolution x-ray studies.

We believe it is significant that the magnetic peak widths for both $USb_{0.8}Te_{0.2}$ and $U_{0.85}Th_{0.15}Sb$ (Ref. 15) are always broader than the experimental resolution. It is important to stress, first that the charge peaks are, by definition, resolution limited, and second that this situation is not found in materials such as Ho and NpAs, both of which also exhibit incommensurate magnetic structures just below T_N. In the case of NpAs the resolution width is attained, at least for the majority of the domains, by 1–2 K below T_N. Doping USb with either Th or Te results in a small perturbation to the underlying lattice. The difference in lattice parameter between USb and UTe, for example, is ~0.6% so that the random strain introduced by a Te atom is easily accommodated. The lattice peaks of these compounds are, as a consequence, sufficiently sharp as to allow an experimental resolution function sharper than the sharpest magnetic features observed. However, on doping USb with either Th or Te, the electronic structure of the compound is changed appreciably by adding one additional electron to the conduction band, with a corresponding change in the valence-band structure. We suggest that these local "perturbations" of the electronic structure are at the origin of the lack of long-range magnetic coherence for both $U_{0.85}Th_{0.15}Te$ and $USb_{0.8}Te_{0.2}$ for all the incommensurate phases below T_N. The perturbation can be thought of as a "smearing" of the sharp features of the Fermi surface that define the incommensurability.

Another interesting effect shown in Fig. 2 and especially in Fig. 7 is that the widths have their minimum close to T_N. This can be understood to result from an interplay between magnetoelastic strain, which favors commensurate magnetic structures, and Fermi surface effects, which are responsible for the incommensurate modulations. At T_N the value of the magnetic moment is a minimum so the strain is small. As the material is cooled the widths of the magnetic peaks increase implying a reduction in the long-range coherence of the incommensurate modulations. This may be understood as being a consequence of the increasing importance of the magnetoelastic strain. The same effect is shown beautifully in the case of holmium; see Fig. 8 of Ref. 27. As noted previously, at lower temperatures close to T_C there is evidence for an actual breakup into several discrete higher-q modulations. Whether these "impurity effects" generated by the addition of tellurium are also responsible for the absence (or at least strong reduction) of the so-called sharp second component[1–6,14] is a matter of speculation. More systematic studies, for example on incommensurate rare-earth alloys, would be useful in this regard.

With both the neutron and x-ray techniques a power-law decay of the bulk magnetization was observed, consistent with an order parameter exponent, β, in either the 3D Heisenberg, or the $n = 6$ $d = 3$, universality class proposed by Mukamel and Krinsky.[17] We have observed magnetic critical scattering up to several degrees above T_N. In the case of the neutron data in particular, the

extracted correlation length exponents, ν, are not consistent with predictions of the universality classes mentioned above. [17,28] We note that the neutron and x-ray experiments show a remarkable degree of consistency in the observed inverse-correlation length critical behavior. Our results may be compared with values of the inverse correlation length exponent ν which have been reported for several cubic-actinide antiferromagnets. In particular, neutron-scattering studies report that for USb[29] $\nu = 0.69 \pm 0.08$, for NpAs[30] $\nu = 0.73 \pm 0.02$, and for PuSb[31] $\nu = 0.58 \pm 0.05$. A previous resonant magnetic x-ray scattering study reports that $\nu = 1.5 \pm 0.3$ for NpAs.[5] The result obtained from our simultaneous fit to both the x-ray and neutron data for $USb_{0.8}Te_{0.2}$ is $\nu = 0.46 \pm 0.3$. The large error is associated with the inclusion of the x-ray data. Considering the neutron results for ν quoted earlier in Sec. III B, it is apparent that the inverse correlation length exponent ν is indeed unexpectedly low for this system.

At T_C our $USb_{0.8}Te_{0.2}$ experiments reveal a discontinuous change in the antiferromagnetic modulation wave vector. The onset of ferromagnetism at T_C is seen clearly by the neutron technique whereas it can only be observed indirectly with x rays through the associated distortion of the charge lattice.

This study illustrates the complementarity of the two techniques of resonant magnetic x-ray scattering and neutron diffraction. The $USb_{0.8}Te_{0.2}$ system is particularly interesting given the unusually large degree of consistency between results obtained by the two techniques.

ACKNOWLEDGMENTS

The authors would like to thank M. Hagen, J.P. Hill, and M.E. Brooks for useful discussions and M.E. Hagen and S.C. Perry for assistance with the data analysis. We are most grateful to D. Gibbs, W. Schoenig, A. Roberts, and S. Coburn for their kind assistance during our synchrotron experiments at the N.S.L.S. We thank Robert Troc of the Institute of Low Temperature Structural Research in Wroclaw, Poland, for his interest and encouragement over a long period of time in research on these materials. We gratefully acknowledge the financial assistance of the S.E.R.C. U.K. and the European Union through the Human Capital and Mobility Program (ERB CHR XCT /930135) and the Large Installation Plan. The National Synchrotron Light Source is supported by the U.S. Department of Energy under Grant No. DE-AC02-76CH00016.

* Present address: European Synchrotron Radiation Facility, BP 220, F38043 Grenoble Cedex, France.

[1] T. R. Thurston, G. Helgesen, J. P. Hill, B. D. Gaulin, and G. Shirane, Phys. Rev. Lett. **70**, 3151 (1993).
[2] T. R. Thurston, G. Helgesen, J. P. Hill, Doon Gibbs, B. D. Gaulin, and P. J. Simpson, Phys. Rev. B **49**, 15 730 (1994).
[3] P. M. Gehring, K. Hirota, C. F. Majkrzak, and G. Shirane, Phys. Rev. Lett. **71**, 1087 (1993).
[4] K. Hirota, G. Shirane, P. M. Gehring, and C. F. Majkrzak, Phys. Rev. B **49**, 11 967 (1994).
[5] S. Langridge, W. G. Stirling, G. H. Lander, and J. Rebizant, Phys. Rev. B **49**, 12 022 (1994).
[6] S. Langridge, W. G. Stirling, G. H. Lander, J. Rebizant, J. C. Spirlet, Doon Gibbs, and O. Vogt, Europhys. Lett. **25**, 137 (1994).
[7] J. Rossat-Mignod, G. H. Lander, and P. Burlet, in *Handbook on the Physics and Chemistry of the Actinides* (North-Holland, Amsterdam, 1985), Vol. 1, p. 415.
[8] P. Burlet, S. Quezel, J. Rossat-Mignod, G. H. Lander, and O. Vogt, J. Magn. Magn. Mater. **14**, 309 (1979).
[9] P. Burlet, S. Quezel, J. Rossat-Mignod, G. H. Lander, and O. Vogt, Physica B **102**, 271 (1980).
[10] F. Hulliger and O. Vogt, Physica B **102**, 316 (1980).
[11] J. C. Spirlet and O. Vogt, in *Handbook on the Physics and Chemistry of the Actinides* (Ref. 7), Vol. 1, p. 79.
[12] D. B. McWhan, C. Vettier, E. D. Isaacs, G. E. Ice, D. P. Siddons, J. B. Hastings, C. Peters, and O. Vogt, Phys. Rev. B **42**, 6007 (1990).
[13] C. C. Tang, W. G. Stirling, G. H. Lander, Doon Gibbs, P. Carra, B. T. Thole, K. Mattenberger, and O. Vogt, Phys. Rev. B **46**, 5287 (1992).
[14] S. Perry *et al.* (unpublished).
[15] J. A. Paixão, G. H. Lander, C. C. Tang, W. G. Stirling, A. Blaise, P. Burlet, P. J. Brown, and O. Vogt, Phys. Rev. B **47**, 8634 (1993).
[16] Hae Seop Shim and B. Lebech, *Annual Progress Report of the Department of Solid State Physics 1 January–31 December 1994* (Risø National Laboratory, Roskilde, 1995), p. 25; J. Rossat-Mignod, P. Burlet, H. Bartholin, J. Villain, W. T. Si, D. Florence, and O. Vogt, Phys. Rev. B **16**, 440 (1977).
[17] D. Mukamel and S. Krinsky, Phys. Rev. B **13**, 5065 (1976).
[18] K. Huang, *Statistical Mechanics* (Wiley, New York, 1987).
[19] S. Langridge, W. G. Stirling, G. H. Lander, and J. Rebizant, Phys. Rev. B **49**, 12 010 (1994).
[20] J. von Boehm and P. Bak, Phys. Rev. Lett. **42**, 122 (1979).
[21] B. Lebech, C. Broholm, K. Clausen, and O. Vogt, J. Magn. Magn. Mater. **54-57**, 505 (1986).
[22] J. Luo, G. T. Trammell, and J. P. Hannon, Phys. Rev. Lett. **71**, 287 (1993).
[23] P. Burlet, D. Bonnisseau, S. Quezel, J. Rossat-Mignod, and J. C. Spirlet, J. Magn. Magn. Mater. **63-64**, 151 (1987).
[24] D. L. Jones, W. G. Stirling, G. H. Lander, J. Rebizant, J. C. Spirlet, M. Alba, and O. Vogt, J. Phys.: Condens. Matter C **3**, 3551 (1991).
[25] J. P. Hill, T. R. Thurston, R. W. Erwin, M. J. Ramstad, and R. J. Birgeneau, Phys. Rev. Lett. **66**, 3281 (1991).
[26] J. P. Hill, Q. Feng, R. J. Birgeneau, and T. R. Thurston, Z. Phys. B **92**, 285 (1993).
[27] G. Helgesen, J. P. Hill, T. R. Thurston, Doon Gibbs, J. Kwo, and M. Hong, Phys. Rev. B **50**, 2990 (1994).
[28] H. E. Stanley, *Introduction to Phase Transitions and Critical Phenomena* (Oxford University Press, New York, 1971).
[29] M. Hagen, W. G. Stirling, and G. H. Lander, Phys. Rev. B **37**, 1846 (1988).
[30] A. T. Aldred, B. D. Dunlap, A. R. Harvey, G. H. Lander, and M. H. Mueller, Phys. Rev. B **9**, 3766 (1974).
[31] P. Burlet, J. Rossat-Mignod, G. H. Lander, J. C. Spirlet, J. Rebizant, and O. Vogt, Phys. Rev. B **36**, 5306 (1987).